J. Fluid Mech. (2021), *vol*. 915, A68, doi:10.1017/jfm.2021.108

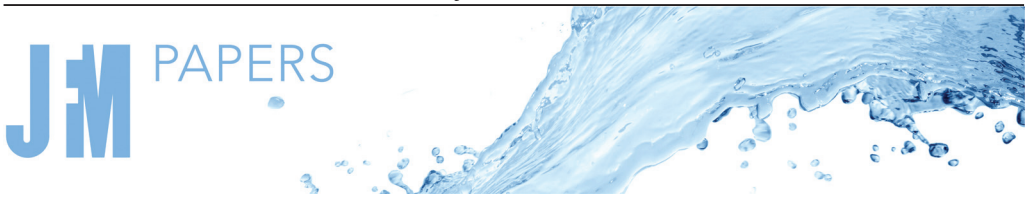

Free-fall velocities and heat transport enhancement in liquid metal magneto-convection

Tobias Vogt[1],†, **Juan-Cheng Yang**[1],[2], **Felix Schindler**[1] **and Sven Eckert**[1]

[1]Institute of Fluid Dynamics, Helmholtz-Zentrum Dresden-Rossendorf, 01328 Dresden, Germany

[2]State Key Laboratory for Strength and Vibration of Mechanical Structures, School of Aerospace, Xi'an Jiaotong University, Xi'an, Shaanxi 710049, PR China

(Received 18 September 2020; revised 10 December 2020; accepted 28 January 2021)

In geo- and astrophysics, low Prandtl number convective flows often interact with magnetic fields. Although a static magnetic field acts as a stabilizing force on such flow fields, we find that self-organized convective flow structures reach an optimal state where the heat transport significantly increases and convective velocities reach the theoretical free-fall limit, i.e. the maximum possible velocity a fluid parcel can achieve when its potential buoyant energy is fully converted into kinetic energy. Our measurements show that the application of a static magnetic field leads to an anisotropic, highly ordered flow structure and a decrease of the turbulent fluctuations. When the magnetic field strength is increased beyond the optimum state, Hartmann braking becomes dominant and leads to a reduction of the heat and momentum transport. The results are relevant for the understanding of magneto-hydrodynamic convective flows in planetary cores and stellar interiors in regions with strong toroidal magnetic fields oriented perpendicular to temperature gradients.

Key words: Bénard convection, magneto convection, MHD turbulence

1. Introduction

Turbulent convective energy coalesces into large coherent flow structures. This is one of the key features that delineates many geo- and astrophysical systems, and also manifests in numerous industrial applications. Often, these systems are subjected to additional, stabilizing forces, such as centrifugal and Coriolis forces due to rotation, or Lorentz forces due to magnetic fields. These forces can substantially affect the flow structures and therefore, the heat and momentum transport of convective systems.

† Email address for correspondence: t.vogt@hzdr.de

The simplest physical model to study thermally driven flows is the so-called Rayleigh–Bénard convection (RBC), where the driving force is a temperature gradient ∇T between a warmer bottom and a cooler top (Ahlers, Grossmann & Lohse 2009; Chillà & Schumacher 2012). An important outcome of RBC studies is the scaling relations for the global heat and momentum transport, expressed non-dimensionally in terms of the Nusselt number (Nu) and Reynolds number (Re), respectively (Grossmann & Lohse 2002; Stevens *et al.* 2013).

When stabilizing forces such as rotation (Guervilly, Hughes & Jones 2014; Stellmach *et al.* 2014), geometrical confinements (Daya & Ecke 2001; Huang *et al.* 2013) or static magnetic fields are added to highly nonlinear systems such as RBC, unexpected features are encountered (Chong *et al.* 2017; Aurnou *et al.* 2018). For instance, studies have shown that rotation around a vertical axis has a strong influence on the flow structure and consequently the heat transport. Although it is well known that the Coriolis force has a stabilizing effect (Proudman 1916; Taylor 1917; Chandrasekhar 1961), it was found that the application of moderate forces can even enhance scalar transport (Rossby 1969; Zhong, Ecke & Steinberg 1993; Liu & Ecke 2009; Stevens *et al.* 2009; Wei, Weiss & Ahlers 2015; Weiss, Wei & Ahlers 2016; Chong *et al.* 2017).

Similarly, magnetic fields exert an influence on electrically conducting fluids by the induction of eddy currents $\boldsymbol{j} = \sigma(\boldsymbol{E} + \boldsymbol{u} \times \boldsymbol{B})$ which give rise to a corresponding Lorentz force $\boldsymbol{f}_l = \boldsymbol{j} \times \boldsymbol{B}$ that acts on the fluid. Here, σ is the electrical conductivity, $\boldsymbol{E}$ is the electric field, $\boldsymbol{u}$ is the velocity and $\boldsymbol{B}$ is the magnetic field. A static magnetic field cannot generate any flow from a quiescent state, however, it can reorganize an electrically conducting flow field so as to minimize the Joule dissipation (Davidson 1995). This is a direct consequence of a reduction of the velocity gradients along the magnetic field direction due to the induced eddy currents (Sommeria & Moreau 1982; Pothérat & Klein 2017).

In thermal convection in liquid metal, the orientation of the applied magnetic field with respect to the temperature gradient ∇T, plays a pivotal role on the details of the resulting flow field. Two field orientations are possible: vertical and horizontal. A vertical magnetic field ($\boldsymbol{B} \parallel \nabla T$) inhibits the onset of liquid metal convection and the heat transport decreases monotonically with increasing magnetic field strength, due to a strong suppression of the bulk flow (Cioni, Chaumat & Sommeria 2000; Aurnou & Olson 2001; Burr & Müller 2001; Liu, Krasnov & Schumacher 2018; Yan *et al.* 2019; Zürner *et al.* 2020). Recently, it was shown that convection in fluid with a Prandtl number $Pr = \nu/\kappa = 8$, whereby ν is the kinematic viscosity and κ is the thermal diffusivity, and under the influence of a vertical magnetic field results in increased heat flux with increasing magnetic field strength but accompanied by a decrease in momentum transport (Lim *et al.* 2019).

A horizontal magnetic field ($\boldsymbol{B} \perp \nabla T$), however, converts the convective motion into a flow pattern of quasi-two-dimensional rolls arranged parallel to the magnetic field (Fauve, Laroche & Libchaber 1981; Busse & Clever 1983; Burr & Müller 2002; Yanagisawa *et al.* 2013; Tasaka *et al.* 2016; Vogt *et al.* 2018*a*).

In this paper, we report on the interaction between liquid metal convection and a static, horizontally imposed magnetic field, which is governed by two non-dimensional parameters. The Rayleigh number

$$Ra = \alpha g \Delta T H^3 / \kappa \nu \tag{1.1}$$

is a measure of the thermal forcing that drives the convection. The strength of the stabilizing Lorentz force due to the applied magnetic field is expressed by the

Chandrasekhar number

$$Q = B^2 L^2 \sigma / \rho \nu = Ha^2. \tag{1.2}$$

Here, H is the distance between the heated and the cooled plates, L is the width of the cell, ΔT is the imposed temperature difference between these plates, B is the strength of the magnetic field, ρ is the density of the liquid metal, α is the thermal expansion coefficient, g denotes the gravitational acceleration, σ is the electrical conductivity and Ha is the Hartmann number.

The present work is a continuation of the work of Vogt *et al.* (2018*a*), where the transition from a three-dimensional to a quasi-two-dimensional flow structure in liquid metal convection under the influence of a horizontal magnetic field was investigated. Vogt *et al.* (2018*a*) focused on the qualitative description of large- and small-scale flow structures at different parametric combinations of Rayleigh number and Chandrasekhar number, while the main goal of this work is to investigate how this transition between flow regimes affects heat and momentum transport. Accordingly, the measuring arrangement at the experiment was extended and the number of measurements was increased significantly to allow a fine increment of the Chandrasekhar number. We find that the reorganization of the convective flow due to the magnetic field results in a significant enhancement of both heat and momentum transport. In the optimum, the convective velocities can even reach the free-fall limit $u_{ff} = \sqrt{\alpha g \Delta T H}$. In classical RBC in fluids with moderate Prandtl numbers, such as water or air, the flow velocities are well below the free-fall limit and do not exceed $u_{max}/u_{ff} \leqslant 0.2$ (Niemela & Sreenivasan 2003). Therefore, our measurements demonstrate how intense low Pr magnetohydrodynamic convective flows can actually become.

2. Laboratory magneto-convection experiments

2.1. *Experimental set-up*

The experiments were conducted at the Helmholtz-Zentrum Dresden Rossendorf (HZDR). The eutectic liquid metal alloy composed of gallium, indium and tin (GaInSn, melting point of $T = 10.5\,^{\circ}$C, $Pr = \nu/\kappa = 0.03$) was used as the working fluid (Plevachuck *et al.* 2014). The liquid metal is contained in an aspect ratio $\Gamma = L/H = 5$ rectangular vessel with a cross-section $L^2 = 200 \times 200$ mm^2 and a height $H = 40$ mm (figure 1). The sidewalls are made of 30 mm thick Polyvinyl chloride and the top and bottom are made of copper. The convection cell is wrapped in 30 mm closed-cell foam to minimize heat loss. The temperature of the top and bottom were adjusted by a constant temperature water bath which flows through channels in the copper plates. The maximum heat flux is 1500 W. The applied temperature drop between the plates is in the range $1.1\ \text{K} \leqslant \Delta T \leqslant 11.7\ \text{K}$ whereby the mean fluid temperature was kept constant at $T_m = 20\,^{\circ}$C. The Rayleigh number is in the range $2.3 \times 10^4 \leqslant Ra \leqslant 2.6 \times 10^5$. A static, uniform horizontal magnetic field penetrates the liquid metal with a strength $0 \leqslant B \leqslant 317$ mT, which gives a Chandrasekhar number range $0 \leqslant Q \leqslant 6.1 \times 10^6$.

The fluid velocities are measured using ultrasound Doppler velocimetry (UDV), which provides instantaneous velocity profiles along two horizontal directions, as shown in figure 1. This technique is useful for non-invasively measuring velocities in opaque fluids (Brito *et al.* 2001; Tsuji *et al.* 2005; Vogt, Räbiger & Eckert 2014; Vogt, Horn & Aurnou 2020). The transducers (TR0805SS, Signal Processing SA) detect the velocity component parallel to the ultrasonic beam with resolutions of approximately 1 mm in the beam direction and 1 Hz in time. One UDV transducer measures the flow velocities perpendicular to the magnetic field ($u_\perp$) and is located in the middle of the cell width at

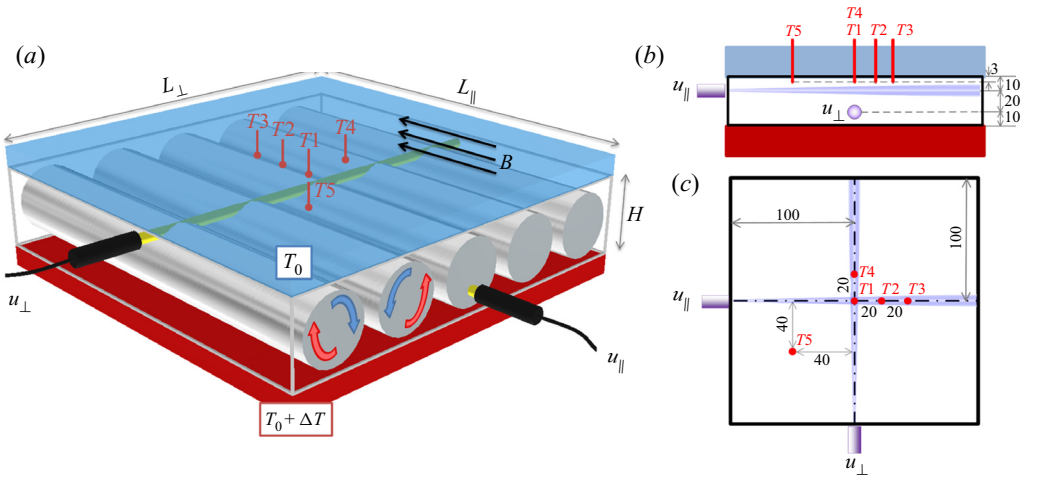

Figure 1. Schematic of the experimental set-up (*a*). The convection rolls (shown in grey), driven by the temperature difference ΔT between the heated bottom plate (red) and the cooled top (blue), are aligned parallel to the magnetic field (B). The velocities ($u_\parallel, u_\perp$) were measured with ultrasound transducers (black tubes) parallel and perpendicular to the direction of the magnetic field. Five thermocouples ($T1$–$T5$) measured the temperature inside the fluid, at a distance of 3 mm from the inner edge of top plate. The side view (*b*) and the top view (*c*) schematics illustrate the positions for the ultrasound transducers and thermocouples. The units are in mm.

$L_\parallel/2$ and 10 mm below the upper boundary ($3H/4$). A second UDV transducer measures the magnetic field parallel velocity component ($u_\parallel$) and is also located in the middle of the cell width at $L_\perp/2$, but at a different height, 10 mm above the lower boundary ($H/4$). Both transducers are in direct contact with the liquid metal which allows a good velocity signal quality even at low velocities.

The difference between the mean temperatures of the heated and the cooled plates is obtained from two sets of nine thermocouples, with each set located in the heated and the cooled plates, respectively. The diameter of the thermocouples is 1.5 mm and they measure the plate temperature at a 2 mm distance from the boundary layer. The temperature difference between the measuring position and the boundary layer due to heat conductivity in the copper was taken into account for the calculation of Ra and Nu. The thermocouples are individually calibrated using a high precision thermometer to ensure accuracy better than 0.05 K.

Another five thermocouples measure the temperature inside the liquid metal at a distance of 3 mm below the cold plate (cf. figure 1*b*,*c*).

The convective heat transport is expressed in dimensionless form by means of the Nusselt number, $Nu = \dot{\Phi}/\dot{\Phi}_{cond}$. Here, $\dot{\Phi}_{cond} = \lambda L^2 \Delta T/H$ is the conductive heat flux, with λ being the thermal conductivity of the liquid metal; $\dot{\Phi} = \rho c_p \dot{V}(T_{in} - T_{out})$ is the total heat flux injected at the bottom and removed from the top wall heat exchanger, whereby c_p is the isobaric heat capacity of water. The total heat flux is determined by the flow rate $\dot{V}$ and the temperature change $(T_{in} - T_{out})$ of the circulating water inside the hot or cold wall heat exchangers.

2.2. *Non-dimensional quantities and characteristic length scale*

The length, velocity and time are made non-dimensional throughout this work using the width L of the cell, the free-fall velocity u_{ff}, and the free-fall time $t_{ff} = H/u_{ff}$, respectively.

In contrast to the work of Vogt *et al.* (2018*a*) the Chandrasekhar number was not determined with the cell height H but with the distance $L_{\parallel}$ of the horizontal walls in the magnetic field direction. The definition of Q using the height H goes back to the studies of Burr & Müller (2002), who used the same definition of the Hartmann number Ha with H as characteristic length for their investigations both in the vertical (Burr & Müller 2001) and the horizontal magnetic field (Burr & Müller 2002). In our opinion, the use of the horizontal dimension of the cell is better suited for the case of a horizontal magnetic field, since the effect of Hartmann braking scales with the dimension of the flow domain in the magnetic field direction (Müller & Bühler 2001; Knaepen & Moreau 2008).

3. Results

All results presented here were recorded after the temperature difference between the hot and the cold plates reached a constant value, and the system had attained thermal equilibrium. At low magnetic field strength, the convection at sufficiently high Ra forms a large-scale circulation with a three-dimensional cellular structure that fills the entire cell (figure 2*a*,*b*,*g*), whereby upwelling takes place in the centre and all four corners of the vessel. A detailed description of this structure can be found in Akashi *et al.* (2019). The large amplitude oscillation that can be seen in figure 2(*a*,*b*) is a typical feature of inertia-dominated liquid metal flows due to their low viscosity and high density (Vogt *et al.* 2018*b*). Applying a horizontal magnetic field to such a three-dimensional flow promotes the formation of quasi-two-dimensional convection rolls that are aligned parallel to the magnetic field lines. The number of rolls formed depends on the ratio between the driving and the stabilizing force Ra/Q and the aspect ratio Γ of the vessel (Tasaka *et al.* 2016). Figure 2(*c*,*d*) shows an example of a convective flow field under the influence of an intermediate magnetic field strength and exhibits an unstable roll configuration. In this range, the magnetic field is not yet intense enough to produce a stable quasi-two-dimensional flow in perfection. The character of the global flow is still three-dimensional, but the magnetic field has caused a breaking of the symmetry, which characterizes the cell structure. The flow structure is dominated by the convection rolls, but their shape and orientation are still transient and subject to strong three-dimensional disturbances. Four rolls are formed in this transitional range, but these are irregular, and temporary changes to three- or five-roll configurations can occur. At higher field strength, the flow develops five counter-rotating convection rolls which are very stable in time (figure 2*e*,*f*,*h*). At this stage, convection has restructured into a quasi-two-dimensional flow field oriented parallel to the magnetic field direction. The symmetric but weak flow that appears along $L_{\parallel}$ is evoked by the Ekman pumping that originates in the Bödewadt boundary layers, where the convection rolls meet the sidewalls (Vogt *et al.* 2018*a*). A weak but regular oscillation is visible in figure 2(*e*,*f*), which is due to inertial waves within the convection rolls (Yang, Vogt & Eckert 2021). However, apart from these regular oscillations, the flow appears to be laminar. Based on the flow fields shown in figure 2, we distinguish here mainly between three characteristic regimes, the 'cell structure', where the influence of the magnetic field on the flow is negligible, the 'unstable 3,4,5-roll' state, where the field starts to reorganize the flow but is not strong enough to form stable roll configurations, and finally the 'stable 5-roll' state at higher Chandrasekhar numbers that results in the formation of stable, quasi-two-dimensional convection rolls.

Figure 3(*a*) shows the root-mean-square (rms) of temperature fluctuations T_{rms} for all three regimes measured with thermocouple $T1$ which is under the cold plate, dipped 3 mm

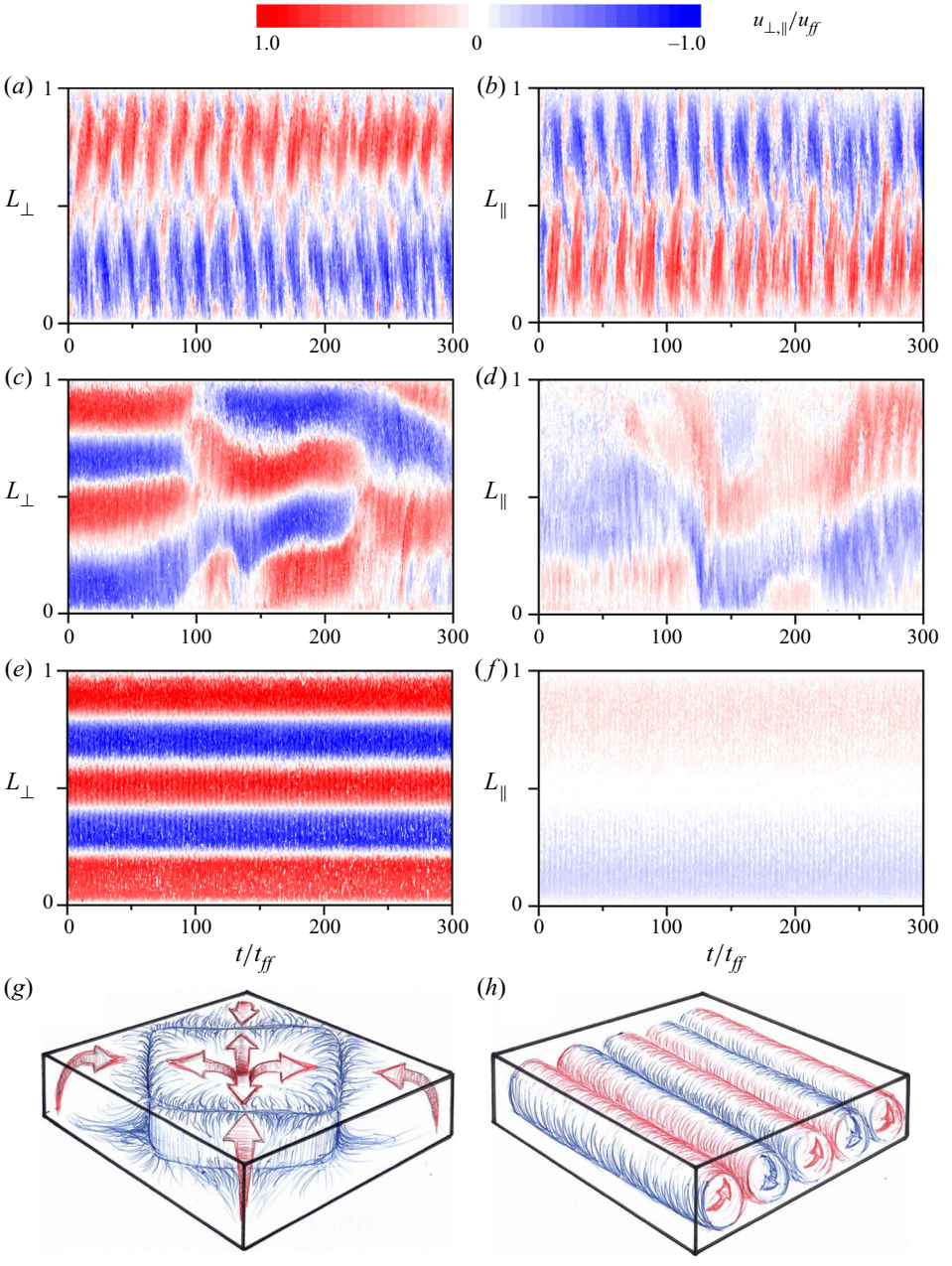

Figure 2. UDV dopplergrams: spatio-temporal distribution of the horizontal velocity measured perpendicular (a,c,e) and parallel (b,d,f) to the magnetic field direction at $Ra = 2.18 \times 10^5$. The measuring lines referred to are indicated in figure 1. A positive (negative) velocity represents a flow away from (towards) the transducer. The velocities and time are non-dimensionalized using the free-fall velocity $u_{ff} = \sqrt{\alpha g \Delta T H} = 21.9$ mm s^{-1} and the free-fall time $t_{ff} = H/u_{ff} = 1.8$ s. The ordinate corresponds to the measuring depth along the horizontal dimensions $L_\perp$ and $L_\parallel$ of the container. An increase of the magnetic field strength changes the global flow structure from: (a,b) oscillating cell structure at $Q = 529$, (c,d) unstable 3,4,5-roll configuration at $Q = 8.7 \times 10^4$, (e,f) stable 5-roll configuration at $Q = 3.8 \times 10^5$. (g) Schematic illustration of the cell regime and (h) the stable 5-role regime. Red areas symbolize warm, ascending fluid and blue areas symbolize colder, descending fluid.

into the liquid metal at the cell centre. The temperature fluctuations are calculated as

$$T_{rms} = \sqrt{\frac{\sum_{t=0}^{t_{end}} (T(t) - T_{avg})^2}{N}}, \tag{3.1}$$

with $T_{avg} = \langle T(t) \rangle_t$ the average over the whole measurement and N the number of measurement points. The vertical dashed lines in figure 3(*b*) show the boundaries between the three different flow regimes. However, this is only indicative since the actual regime boundaries depend not only on Q but also on Ra. The fluctuations are strongest in the cell structure regime and the unstable 3,4,5-roll regime. The larger the Ra number, the stronger the fluctuations. At the transition to the stable 5-roll regime, the fluctuations decrease significantly and are close to zero, which indicates that, from this point on, the position and orientation of the rolls within the convection cell are arrested by the applied magnetic field. The slight but systematic increase of the fluctuations in the stable regime is surprising at first sight, but can be explained by the occurrence of inertial waves inside the convection rolls (Yang *et al.* 2021). Finally, at very high magnetic field strengths, these oscillations are also damped and the temperature fluctuations decrease again and approach zero. Figure 3(*b*) shows the cross-correlation of the different temperature sensors within the liquid metal calculated as

$$R_{i,j} = \frac{\sum_{t=0}^{t_{end}} (T_i(t) - T_{i,avg})(T_j(t) - T_{j,avg})}{\sqrt{\sum_{t=0}^{t_{end}} (T_i(t) - T_{i,avg})^2} \sqrt{\sum_{t=0}^{t_{end}} (T_j(t) - T_{j,avg})^2}} \tag{3.2}$$

where $R_{i,j}$ is Pearson's correlation coefficient. In the cell structure regime, all cross-correlation coefficients are scattered around zero and indicate a negligible correlation between the different measurement points due to a complex and turbulent flow field. In the unstable roll regime, the first rolls form along the magnetic field and the cross-correlation coefficient between the corresponding adjacent sensors in the magnetic field direction increases and approaches $R_{i,j} \approx 1$.

In the stable 5-roll regime, sensors $T1$, $T2$ and $T3$ are located along the same roll. The sensor $T5$ is located centrally above the neighbouring convection roll with opposite rotation direction. Sensor $T4$ is located centrally between two neighbouring convection rolls.

During transition to the stable 5-roll regime, the values for $R_{T1\text{–}T2}$ and $R_{T1\text{–}T3}$ decrease initially, and then approach a value of 1 again. A correlation of approximately 1 is expected as these thermocouples ($T1$, $T2$ and $T3$) are located along the same roll. The reason for the initial decrease of the cross-correlation coefficient is that the oscillations at the beginning of the stable roll regime are still weak and three-dimensional in nature (Yang *et al.* 2021). With increasing magnetic field strength, the three-dimensional character of the oscillations is suppressed, and from $Q > 10^6$ onwards, only quasi-two-dimensional oscillations take place. The cross-correlation coefficient of $R_{T1\text{–}T2}$ and $R_{T1\text{–}T3}$ then reaches its maximum. The oscillations of neighbouring rolls take place with a phase shift of π. For this reason, $T5$ which is located centrally above the neighbouring roll with an opposite direction of rotation, registers a cross-correlation coefficient $R_{T1\text{–}T5} \approx -1$. At the measuring position $T4$ between two adjacent rolls, remaining oscillations vanish with increasing Q and the correlation coefficient $R_{T1\text{–}T4}$ approaches zero for high magnetic field strengths.

For the case of RBC without a magnetic field, our measurements show that the heat transport properties scale as: $Nu_0 = (0.166 \pm 0.014) Ra^{0.250 \pm 0.007}$, as shown in

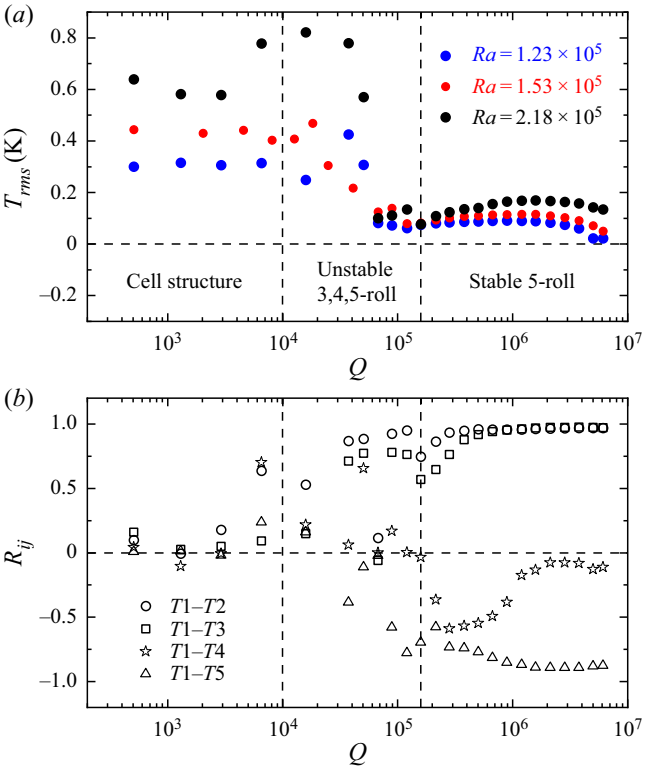

Figure 3. Liquid metal temperature measurements at a 3 mm distance from the top plate and their dependence on Q. (*a*) The rms of the temperature fluctuation of $T1$ for three different Ra numbers. (*b*) Cross-correlation coefficient at different temperature measuring positions at $Ra = 2.18 \times 10^5$. The different symbols denote the value of the cross-correlation coefficients between corresponding thermocouples: $T1$ and $T2$ (circles), $T1$ and $T3$ (squares), $T1$ and $T4$ (stars) and $T1$ and $T5$ (triangles).

figure 4(*a*). This is in reasonable agreement with $Nu_0 = 0.147Ra^{0.257}$ measured in mercury (Rossby 1969) and $Nu_0 = 0.19Ra^{0.249}$ measured in gallium (King & Aurnou 2013). Note, that mercury, gallium and GaInSn have comparable Prandtl numbers in the range $Pr = 0.025$–0.033. The good agreement between the measured Nu numbers on the top and bottom shows that the heat loss is negligible. Figure 4(*b*) presents the relative deviation $(Nu–Nu_0)/Nu_0$ for convection with an imposed magnetic field, where Nu_0 is the corresponding Nusselt number for RBC (without a magnetic field). In the case of cellular flow structures, which are the prevailing structures for $0 < Q < 1 \times 10^4$, the heat transfer does not vary remarkably with increasing Q. This behaviour changes in the range $1 \times 10^4 < Q < 1.6 \times 10^5$, where the formation of unstable convection rolls proceeds with a significant increase of heat transfer. Finally, for $Q > 1.6 \times 10^5$, Nu reaches a maximum before the heat transfer decreases for even higher Q. The investigation of a wider Ra range is not possible with our current experimental set-up. This is due to limited power range of the thermostats, and the cell height which limits Rayleigh number, $Ra_{max} \approx 3 \times 10^5$. On the other hand, lowering $Ra \leqslant 10^5$ triggers a transition from a stable 5-roll to a 4-roll structure regime which is beyond the scope of this paper, as we focus only on the Ra range where the stable 5-roll configuration fits well into the aspect ratio $\Gamma = 5$ of the cell. Enhancement of heat transfer in a liquid metal layer due to the application of a horizontal

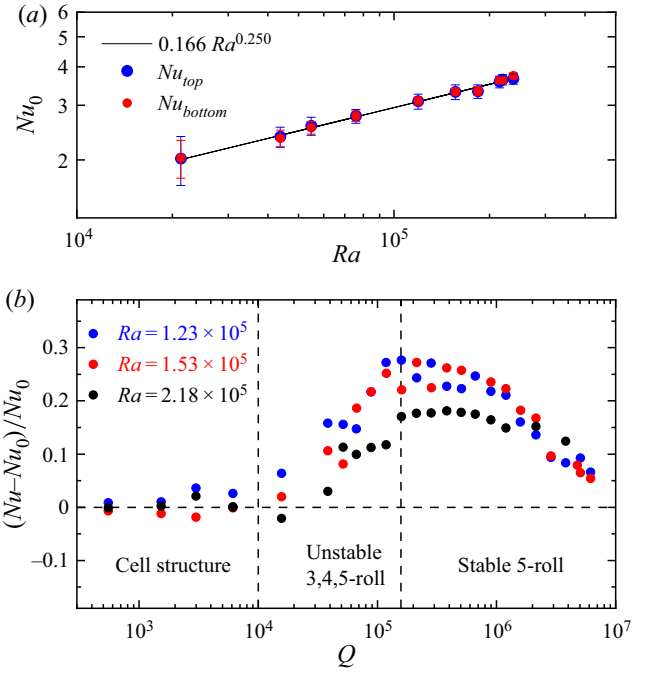

Figure 4. (*a*) Measured Nusselt number Nu_0 for convection without magnetic field. Here, Nu_{top} and Nu_{bottom} are based on the total heat flux measured at the top and bottom heat exchanger, respectively. The error bars show the measured standard deviation. (*b*) Relative deviations of the heat transfer from the reference state of RBC (without a magnetic field), $(Nu–Nu_0)/Nu_0$ as a function of Q for three different Ra numbers. The heat transfer reaches its maximum at $Q \approx 2.5 \times 10^5$ when the magnetic field forms stable convection rolls aligned parallel to the magnetic field.

magnetic field was also investigated by Burr & Müller (2002). Temperature measurements revealed an increase of Nu in a certain range of Q. The correlation of temperature signals suggests that the enhancement of the convective heat transfer is accompanied by the existence of non-isotropic time-dependent flows. However, there are still no direct flow measurements of this phenomenon to explain the increase in convective heat transport.

Based on velocity measurements, we analyse the Q dependence of the amplitude of the velocity components perpendicular $\hat{u}_\perp$ and parallel $\hat{u}_\parallel$ to the magnetic field as shown in figure 5. The maximum velocity values $\hat{u}_i$ for figure 5 were determined as follows: for each measurement, a velocity threshold was defined, such that 95 % of the velocity values of a measurement are below the threshold value. This approach provides very reliable values for the vast majority of measurements. Only at the largest Q and the associated very low velocities $\hat{u}_\parallel$, is the signal-to-noise ratio of the velocity measurements not sufficient to apply this method. For these measurements, $\hat{u}_\parallel$ was determined from the time-averaged quasi-stationary velocity profile.

The flow velocities, and as such the Re number, increases with Ra in all three regimes. As for the heat transfer, the velocity components of the cell structure do not significantly change for $Q < 1 \times 10^4$. Both velocity components, $\hat{u}_\perp$ and $\hat{u}_\parallel$, are of the same order of magnitude and reach an amplitude of approximately $\hat{u}_\perp/u_{ff} \approx 0.7$, which is an expected velocity value for low Pr thermal convection in this Ra range (Vogt *et al.* 2018*b*; Zürner *et al.* 2019). For $Q > 1 \times 10^4$, the development of the unstable 3,4,5-roll state goes along with a separation of the velocity components. The increase of $\hat{u}_\perp$ and the decrease of $\hat{u}_\parallel$

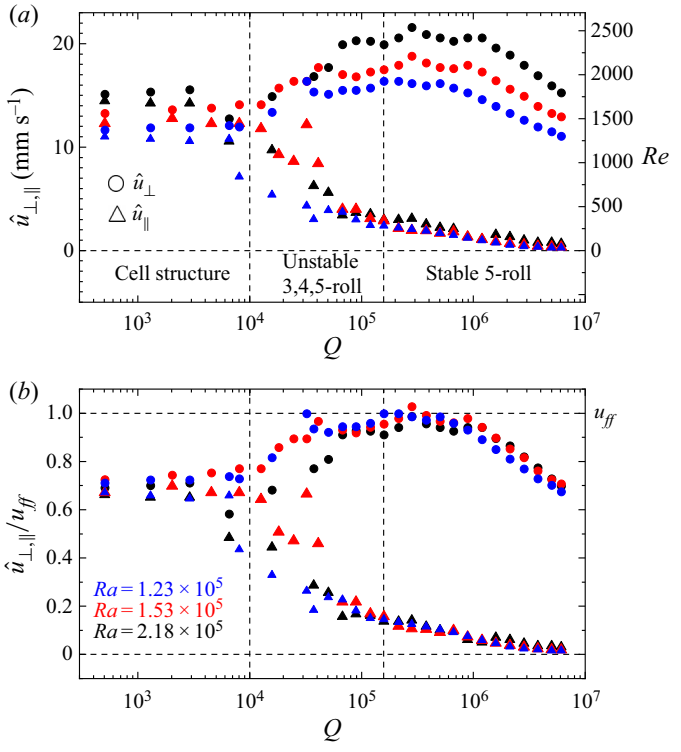

Figure 5. (*a*) The Q dependence of the $\hat{u}_\perp$ and $\hat{u}_\parallel$ velocity components and the corresponding Reynolds number $Re = \hat{u}_i H/\nu$. (*b*) The Q dependence of the normalized horizontal velocity amplitudes for three different Ra numbers. The field-normal velocity amplitude increases from $\hat{u}_\perp/u_{ff} \approx 0.7$ for cellular flow structures ($Q < 1 \times 10^4$) to $O(u_{ff})$ in the stable 5-roll regime ($Q \approx 2.5 \times 10^5$). The diverging branches of $\hat{u}_\parallel$ and $\hat{u}_\perp$ start with the transition from a cellular flow structure to magnetic field aligned convection rolls at $Q > 1 \times 10^4$.

indicate that the flow field starts to become quasi-two-dimensional. The relatively large scatter of the velocity data in this regime is caused by the transient flow behaviour with frequent reversals of the flow direction. At $Q > 1.6 \times 10^5$, the flow structure changes into the stable 5-roll state, which remains the dominant flow structure for at least one decade of Q numbers. The small scattering of the measured velocity amplitudes in this regime reflects the stable characteristic of this flow configuration. The velocity component parallel to the magnetic field $\hat{u}_\parallel$ decreases monotonically for higher Q while $\hat{u}_\perp$ reaches a maximum around $Q \approx 2.5 \times 10^5$, where the velocity amplitudes reach the theoretical free-fall limit u_{ff}. The normalization of the velocity amplitude with the free-fall velocity yields good conformity for the different Ra.

4. Discussion

We have demonstrated that the rearrangement of a three-dimensional thermal convection flow into a quasi-two-dimensional flow field, due to an applied static magnetic field, results in significantly increased heat and momentum transport. The convection forms five counter-rotating rolls, whereby the diameter of the rolls corresponds to the height of the fluid layer and the number of rolls results from the aspect ratio $\Gamma = 5$ of the vessel. The preferred orientation of the rolls implies that momentum oriented parallel to the magnetic

field is redirected in the direction perpendicular to the field. Therefore, $\hat{u}_{\parallel}$ decreases while $\hat{u}_{\perp}$ increases. In addition, the intensity of fluctuations in the temperature and velocity fields decreases and the stabilized convection rolls appear laminar and quasi-stationary.

The vertical velocity component u_z is responsible for convective heat flux, but this component was not directly measured in the experiment. However, our measurements show a fully three-dimensional flow in the cell structure regime wherein the three velocity components are of similar amplitude. It can therefore be assumed that the velocity components in this regime are as follows: $u_z \approx u_{\perp} \approx u_{\parallel} \approx 0.7u_{ff}$. By contrast, in the quasi-two-dimensional, stable 5-roll regime, the flow component parallel to the magnetic field was measured to be significantly weaker compared to the flow component perpendicular to the magnetic field. These experimental results, in conjunction with the prevailing topology of the flow structure, and the requirement imposed by continuity indicate that the following relation would hold for the velocity components at the optimal state of the stable 5-roll regime: $u_z \approx u_{\perp} \approx u_{ff}$.

In classical RBC in fluids with moderate Prandtl numbers, such as water or air, the flow velocities are well below the free-fall limit and never exceed $u_{max}/u_{ff} \leqslant 0.2$ (Niemela & Sreenivasan 2003). Our results show unequivocally that the flow has a predisposition to reorient itself perpendicular to the magnetic field, which allows it to attain the optimal state wherein the fluid parcel traverses with the maximum possible velocity, the free-fall velocity. Consequently, the vigour of the convective flow in such a state is intense, leading to an enhancement of the heat flux. Further increase of the Lorentz force or Q, beyond the optimum state yields reduced convective transport due to the increasing dominance of the Hartmann braking in the lateral boundary layers perpendicular to the magnetic field (Vogt *et al.* 2018*a*; Yang *et al.* 2021). In an infinite fluid layer, the Hartmann braking for an ideal two-dimensional flow structure aligned with the magnetic field direction would disappear since the characteristic Hartmann damping time scale $\tau_{HB} = \sqrt{\rho L^2/\sigma \nu B^2}$ shows a linear dependence on the distance L between the Hartmann walls (Sommeria & Moreau 1982).

In previous works (Chong *et al.* 2017; Lim *et al.* 2019), the increase in Nusselt number was explained as a result of increased coherency of the flow structures, which act as the main carrier for the heat transport. Moreover, the authors concluded that the maximum heat flux is achieved when the thermal and viscous boundary layers reach the same thickness. Our results differ in several respects from the studies mentioned above. First, the low $Pr \ll 1$ implies that the viscous boundary layer is always nested well inside the much thicker thermal boundary layer. A cross-over of the boundary layer thicknesses is, therefore, not expected in very low Prandtl number fluids such as liquid metals. Second, in our case, not only the heat flux, but also the momentum transport perpendicular to the magnetic field, is increased. And finally, the low Pr of liquid metals implies that the Péclet number $Pe = Re\,Pr$ remains low when compared to moderate Pr flows at a comparable turbulence level (Vogt *et al.* 2018*b*). The consequence is a pronounced coherence in the flow field even without the influence of the magnetic field.

The application of a horizontal magnetic field supports an increase in the coherence of the flow pattern in a particularly striking way by transforming unsteady three-dimensional flows into stable two-dimensional structures. In this context, it is very interesting to point out that the application of small magnetic fields in the range of the three-dimensional flow ($Q < 10^4$) does not show any measurable effects for the heat and momentum transport. From magnetohydrodynamic (MHD) turbulence, it is known that the transition from isotropic to anisotropic turbulence starts at values of the magnetic interaction parameter $N = Q/Re \approx 1$ (Davidson 1995; Eckert *et al.* 2001). When crossing this threshold, the effect of the Lorentz force sets in, which prevents three-dimensional structures from

absorbing the energy supplied by the thermal driving. Instead, the development of quasi-two-dimensional structures is promoted. The interaction parameter reaches values of approximately 5 at the transition from the cell structure to the unstable roll regimes. The cell structure is completely three-dimensional and an amplification of the flow by the Lorentz force is not plausible in view of the described mechanism. Only with the emergence of the convection rolls are the quasi-two-dimensional structures available, into which energy can be transferred. Accordingly, our measurements show a simultaneous increase of both momentum and heat transport in the regime of unstable roll structures.

In conclusion, we have shown how a stabilizing, static magnetic field can significantly alter the flow dynamics such that the free-fall velocity is attained by the flow structure, resulting in enhanced heat and momentum transport in thermal convection. These trends remain a consistent feature for all the Rayleigh numbers investigated. It is likely that the optimum state for the heat and momentum transport does not solely depend on Q, but also on a combination of Q, Ra and Γ. Further investigation of this phenomenon with other combinations of parameters would therefore be desirable.

Acknowledgements. The authors thank S. Singh, M. Akashi, J. Aurnou, S. Horn, T. Yanagisawa, Y. Tasaka and S. Su for fruitful discussions.

Funding. This work is supported by the Priority Programme SPP 1881 Turbulent Superstructures of the Deutsche Forschungsgemeinschaft (DFG) under the grant VO 2331/3. T.V. and F.S. also thank the DFG for the support under the grant VO 2331/1. The contribution of J.C.Y. in this project is financially supported by CSC (China Scholarship Council).

Declaration of interests. The authors report no conflict of interest.

Author ORCIDs.
Tobias Vogt https://orcid.org/0000-0002-0022-5758;
Juan-Cheng Yang https://orcid.org/0000-0002-5834-5680;
Felix Schindler https://orcid.org/0000-0003-2123-0430;
Sven Eckert https://orcid.org/0000-0003-1639-5417.

Author contributions. T.V. and J.C.Y. contributed equally to this work and should be considered joint first authors. T.V. and S.E. planned and designed research; T.V., J.C.Y. and F.S. performed research; T.V., J.C.Y., F.S. and S.E. analysed data; T.V., J.C.Y., F.S. and S.E. wrote the paper.

References

Ahlers, G., Grossmann, S. & Lohse, D. 2009 Heat transfer and large scale dynamics in turbulent Rayleigh–Bénard convection. *J. Fluid Mech.* **5**, 113–133.

Akashi, M., Yanagisawa, T., Tasaka, Y., Vogt, T., Murai, Y. & Eckert, S. 2019 Transition from convection rolls to large-scale cellular structures in turbulent Rayleigh–Bénard convection in a liquid metal layer. *Phys. Rev. Fluids* **4**, 033501.

Aurnou, J. & Olson, P. 2001 Experiments on Rayleigh–Bénard convection, magnetoconvection and rotating magnetoconvection in liquid gallium. *J. Fluid Mech.* **430**, 283–307.

Aurnou, J., Bertin, V., Grannan, A., Horn, S. & Vogt, T. 2018 Rotating thermal convection in liquid gallium: multi-modal flow, absent steady columns. *J. Fluid Mech.* **846**, 846–876.

Brito, D., Nataf, C., Cardin, P., Aubert, J. & Masson, J.P. 2001 Ultrasonic Doppler velocimetry in liquid gallium. *Exp. Fluids* **31**, 653–663.

Burr, U. & Müller, U. 2001 Rayleigh–Bénard convection in liquid metal layers under the influence of a vertical magnetic field. *Phys. Fluids* **13**, 3247–3257.

Burr, U. & Müller, U. 2002 Rayleigh–Bénard convection in liquid metal layers under the influence of a horizontal magnetic field. *J. Fluid Mech.* **453**, 345–369.

Busse, F.H. & Clever, R.M. 1983 Stability of convection rolls in the presence of a horizontal magnetic field. *J. Theor. Appl. Mech.* **2**, 495–502.

Chandrasekhar, S. 1961 *Hydromagnetic and Hydrodynamic Stability*. Oxford University Press.

CHILLÀ, F. & SCHUMACHER, J. 2012 New perspectives in turbulent Rayleigh–Bénard convection. *Eur. Phys. J.* E **35**, 58.

CHONG, K.L., YANG, Y., HUANG, S.D., ZHONG, J.Q., STEVENS, R.J.A.M., VERZICCO, R., LOHSE, D. & XIA, K.Q. 2017 Confined Rayleigh–Bénard, rotating Rayleigh–Bénard, and double diffusive convection: a unifying view on turbulent transport enhancement through coherent structure manipulation. *Phys. Rev. Lett.* **119**, 064501.

CIONI, S., CHAUMAT, S. & SOMMERIA, J. 2000 Effect of a vertical magnetic field on turbulent Rayleigh–Bénard convection. *Phys. Rev.* E **62**, R4520.

DAVIDSON, P. 1995 Magnetic damping of jets and vortices. *J. Fluid Mech.* **299**, 153–186.

DAYA, Z.A. & ECKE, R.E. 2001 Does turbulent convection feel the shape of the container? *Phys. Rev. Lett.* **87**, 184501.

ECKERT, S., GERBETH, G., WITKE, W. & LANGENBRUNNER, H. 2001 MHD turbulence measurements in a sodium channel flow exposed to a transverse magnetic field. *Intl J. Heat Fluid Flow* **22**, 358–364.

FAUVE, S., LAROCHE, C. & LIBCHABER, A. 1981 Effect of a horizontal magnetic field on convective instabilities in mercury. *J. Phys. Lett.* **42**, L455.

GROSSMANN, S. & LOHSE, D. 2002 Prandtl and Rayleigh number dependence of the Reynolds number in turbulent thermal convection. *Phys. Rev.* E **66**, 016305.

GUERVILLY, C., HUGHES, D.W. & JONES, C.A. 2014 Large-scale vortices in rapidly rotating Rayleigh–Bénard convection. *J. Fluid Mech.* **758**, 407–435.

HUANG, S.D., KACZOROWSKI, M., NI, R. & XIA, K.Q. 2013 Confinement-induced heat-transport enhancement in turbulent thermal convection. *Phys. Rev. Lett.* **111**, 104501.

KING, E. & AURNOU, J. 2013 Turbulent convection in liquid metal with and without rotation. *Proc. Natl Acad. Sci. USA* **110**, 6688.

KNAEPEN, B. & MOREAU, R. 2008 Magnetohydrodynamic turbulence at low magnetic Reynolds number. *Annu. Rev. Fluid Mech.* **40**, 25–45.

LIM, Z., CHONG, K., DING, G. & XIA, K.Q. 2019 Quasistatic magnetoconvection: heat transport enhancement and boundary layer crossing. *J. Fluid Mech.* **870**, 519–542.

LIU, Y. & ECKE, R.E. 2009 Heat transport measurements in turbulent rotating Rayleigh–Bénard convection. *Phys. Rev.* E **80**, 036314.

LIU, W., KRASNOV, D. & SCHUMACHER, J. 2018 Wall modes in magnetoconvection at high Hartmann numbers. *J. Fluid Mech.* **849**, R2.

MÜLLER, U. & BÜHLER, U. 2001 *Magnetofluiddynamics in Channels and Containers*. Springer.

NIEMELA, J.J. & SREENIVASAN, K.R. 2003 Rayleigh-number evolution of large-scale coherent motion in turbulent convection. *Eur. Phys. Lett.* **62**, 829–833.

PLEVACHUCK, Y., SKLYARCHUK, V., ECKERT, S., GERBETH, G. & NOVAKOVIC, R. 2014 Thermophysical properties of the liquid Ga–In–Sn eutectic alloy. *J. Chem. Engng Data* **59**, 757–763.

POTHÉRAT, A. & KLEIN, R. 2017 Do magnetic fields enhance turbulence at low magnetic Reynolds number? *Phys. Rev. Fluids* **2**, 063702.

PROUDMAN, J. 1916 On the motion of solids in a liquid possessing vorticity. *Proc. R. Soc. Lond.* A **92**, 408–424.

ROSSBY, H. 1969 A study of Bénard convection with and without rotation. *J. Fluid Mech.* **36**, 309–335.

SOMMERIA, J. & MOREAU, R. 1982 Why, how, and when, MHD turbulence becomes two-dimensional. *J. Fluid Mech.* **118**, 507–518.

STELLMACH, S., LISCHPER, M., JULIEN, K., VASIL, G., CHENG, J.S., RIBEIRO, A., KING, E.M. & AURNOU, J.M. 2014 Approaching the asymptotic regime of rapidly rotating convection: boundary layers versus interior dynamics. *Phys. Rev. Lett.* **113**, 254501.

STEVENS, R.J.A.M., ZHONG, J.Q., CLERCX, H.J.H., AHLERS, G. & LOHSE, D. 2009 Transitions between turbulent states in rotating Rayleigh–Bénard convection. *Phys. Rev. Lett.* **103**, 024503.

STEVENS, R., POEL, E., GROSSMANN, S. & LOHSE, S. 2013 The unifying theory of scaling in thermal convection: the updated prefactors. *J. Fluid Mech.* **730**, 295–308.

TASAKA, Y., IGAKI, K., YANAGISAWA, T., VOGT, T., ZÜRNER, T. & ECKERT, S. 2016 Regular flow reversals in Rayleigh–Bénard convection in a horizontal magnetic field. *Phys. Rev.* E **93**, 043109.

TAYLOR, G. 1917 Motion of solids in fluids when the flow is not irrotational. *Proc. R. Soc. Lond.* A **93**, 99–113.

TSUJI, Y., MIZUNO, T., MASHIKO, T. & SANO, M. 2005 Mean wind in convective turbulence of mercury. *J. Phys. Lett.* **94**, 034501.

VOGT, T., RÄBIGER, D. & ECKERT, S. 2014 Inertial wave dynamics in a rotating liquid metal. *J. Fluid Mech.* **753**, 472–498.

VOGT, T., ISHIMI, W., YANAGISAWA, T., TASAKA, Y., SAKURABA, A. & ECKERT, S. 2018*a* Transition between quasi-two-dimensional and three-dimensional Rayleigh–Bénard convection in a horizontal magnetic field. *Phys. Rev. Fluids* **3**, 013503.

VOGT, T., HORN, S., GRANNAN, A. & AURNOU, J. 2018*b* Jump rope vortex in liquid metal convection. *Proc. Natl Acad. Sci. USA* **115**, 12674.

VOGT, T., HORN, S. & AURNOU, J. 2020 Oscillatory thermal-inertial flows in rotating liquid metal convection. *J. Fluid Mech.* **911**, A5.

WEI, P., WEISS, S. & AHLERS, G. 2015 Multiple transitions in rotating turbulent Rayleigh–Bénard convection. *Phys. Rev. Lett.* **114**, 114506.

WEISS, S., WEI, P. & AHLERS, G. 2016 Heat-transport enhancement in rotating turbulent Rayleigh–Bénard convection. *Phys. Rev.* E **93**, 043102.

YAN, M., CALKINS, M.A., MAFFEI, S., JULIEN, K., TOBIAS, S.M. & MARTI, P. 2019 Heat transfer and flow regimes in quasi-static magnetoconvection with a vertical magnetic field. *J. Fluid Mech.* **877**, 1186–1206.

YANAGISAWA, T., HAMANO, Y., MIYAGOSHI, T., YAMAGISHI, Y., TASAKA, Y. & TAKEDA, Y. 2013 Convection patterns in a liquid metal under an imposed horizontal magnetic field. *Phys. Rev.* E **88**, 063020.

YANG, J.C., VOGT, T. & ECKERT, S. 2021 Transition from steady to oscillating convection rolls in Rayleigh–Bénard convection under the influence of a horizontal magnetic field. *Phys. Rev. Fluids* **6**, 023502.

ZHONG, F., ECKE, R.E. & STEINBERG, V. 1993 Rotating Rayleigh–Bénard convection: asymmetric modes and vortex states. *J. Fluid Mech.* **249**, 135–159.

ZÜRNER, T., SCHINDLER, F., VOGT, T., ECKERT, S. & SCHUMACHER, J. 2019 Combined measurement of velocity and temperature in liquid metal convection. *J. Fluid Mech.* **876**, 1108–1128.

ZÜRNER, T., SCHINDLER, F., VOGT, T., ECKERT, S. & SCHUMACHER, J. 2020 Flow regimes of Rayleigh–Bénard convection in a vertical magnetic field. *J. Fluid Mech.* **894**, A21.